PHYSICAL REVIEW B **83**, 184120 (2011)

Classification of laminate domain patterns in ferroelectrics

N. T. Tsou,* P. R. Potnis,† and J. E. Huber‡

Department of Engineering Science, University of Oxford, Parks Rd.,Oxford OX1 3PJ, United Kingdom

(Received 6 March 2011; revised manuscript received 8 April 2011; published 31 May 2011)

Ferroelectric crystals are known to adopt low-energy, compatible domain configurations. Observations show that these configurations are commonly multirank laminate patterns. In this work, a method to classify and enumerate the laminate domain patterns that can form is presented. The criteria of exact compatibility for laminates structures in a ferroelectric single crystal are used to find all the rank-2 arrangements of domains in the polar tetragonal crystal system. Surprisingly, only eight distinct rank-2 laminate patterns that satisfy compatibility conditions at all domain walls are found. These patterns are classified and correlated with observations of domains in single crystals, showing good agreement.

DOI: 10.1103/PhysRevB.83.184120 PACS number(s): 03.65.Vf, 64.60.Bd

I. INTRODUCTION

The domain structure in ferroelectric single crystals is a crucial factor that determines macroscopic properties. Observations show that domains typically form multirank laminate structures, such as the well-known herringbone and stripe patterns, which result from twinning to minimize the overall energy of the crystal.[1–3] These patterns are significant in bulk materials because the geometric arrangement of domains controls the macroscopic material properties, such as piezoelectric coefficients, elastic moduli, and dielectric permittivity.[4,5] Moreover, the ferroelectric switching behavior is strongly dependent on the domain pattern.[6–9] At the microscopic and nanoscale, thin-film ferroelectrics also show compatible domain patterning,[10–13] and again it is found that the domain pattern strongly influences material responses, for example, the thermal stability[14–18] and achievable remanent polarization.[19] Given the great number of publications reporting observations of particular domain patterns, it is remarkable that there is up to now no systematic classification of these patterns. What periodic arrangements of domains are possible? Of these, which are minimum energy states? What is the relationship between the underlying crystal structure and the domain patterns that form? In the present work, we set out a method for determining the compatible arrangements of domains that can form in a given crystal system, and illustrate the power of this method with a detailed study of polar tetragonal crystals. The approach is sufficiently general to permit extension to other ferroelectric crystal systems as well as multiferroics and shape memory materials.

The formation of domain patterns in ferroelectrics is well explained by the constrained theory,[20,21] which assumes that material points adopt minimum energy states of a multiwell potential. The central result is that where a pair of domains meet, the domain wall adopts an orientation which satisfies compatibility conditions. Many theoretical models use the compatibility equations, which are an analog of the twinning equation for martensites, to predict domain patterns in ferroelectric crystals.[4,8,22] The models proposed by Li and Liu[4] and Yen *et al.*[8] focus on specific domain laminate arrangements which satisfy compatibility equations between laminate composites *averagely*. Then, the assumption of a fine phase mixture, with a separation of length scales between successive laminations,[20] is necessary to ensure energy minimization. However, observations of domains in single crystal ferroelectrics suggest that these materials commonly adopt structures in which successive levels of lamination occur with similar domain wall spacing—that is, no separation of length scale. For such structures to minimize energy within the constrained theory, it is necessary that the compatibility equations are satisfied at every junction of domains. Tsou and Huber[22] have identified *exact* compatibility conditions for laminates and used these conditions to find laminate domain arrangements that can form under given strain and polarization boundary conditions.

It is of interest to compare the constrained theory with other physical models, such as the time-dependent Ginzburg-Landau (TDGL) theory,[23,24] which is one of the most widely used approaches. Models using the TDGL theory[6,25–28] treat the domain wall as a diffuse interface and by adopting periodic boundary conditions can find periodic domain patterns. For given initial conditions, a TDGL simulation generates a unique equilibrium solution. Since the domain walls in ferroelectrics are thin (generally a few lattice parameters[29]), the patterns generated by TDGL models typically satisfy the compatibility conditions of the constrained theory, either averagely or exactly. Thus, they closely match the patterns generated by sharp interface models using the constrained theory. However, the simplicity of the sharp interface models makes it possible to find all of the compatible domain patterns which satisfy a given set of boundary conditions.[19,22] By removing the boundary conditions altogether, a further step can be taken: the entire set of compatible domain arrangements can be enumerated. Hence, an advantage of the constrained theory is the opportunity to obtain an overview of the set of domain patterns that may form. This is the approach pursued in the present work, subject to the restriction that we consider only those patterns that can be classified as periodic multirank laminates.

An exactly compatible laminate structure has one-to-one perfect matching of domains, such that wherever domains meet, there is no incompatibility. In a multirank laminate, this can be achieved provided: (i) laminations have matched domain wall spacings wherever they meet, (ii) laminations have aligned domain wall orientations wherever they meet, and (iii) each pair of adjacent domains satisfies the compatibility equations.[22] These conditions are further explained and restated in algebraic form in Sec. II.

Observations[1,3,30] and theoretical models[5,19,21,22,31] show a variety of exactly compatible laminate structures, particularly of rank 2. Thus, it is natural to seek the set of rank-2 laminate structures that can form. A knowledge of the set of possible structures is helpful for several reasons: First, it assists in the interpretation of microstructure observations. For example, images obtained through microscopy give a two-dimensional view and commonly present ambiguity between domain types. Secondly, it is desirable to optimize material properties and structures for technological applications. A knowledge of the possible domain arrangements can be used to design future materials with optimum performance. Domain engineering can be achieved through bulk-scale processing, or by manipulation of domains using tools, such as the atomic force microscope. For example, Balke *et al.*[32] recently demonstrated the ability to nucleate domains in $BiFeO_3$ by scanning probe methods. Several recent works report observations of domain patterns and their dynamics using methods, such as atomic force microscopy (AFM) and piezoresponse force microscopy (PFM).[33–35] However, the classification of such patterns has not been tackled previously. Consequently, the insight provided by having an overview of the set of possible patterns is currently not available from the literature.

In order to identify the set of possible rank-2 laminate domain patterns, we utilize the exact compatibility conditions to evaluate all periodic laminates in the polar tetragonal crystal system. Surprisingly, just eight distinct types of compatible rank-2 domain topology can form. This family of structures is classified, and observations of barium titanate ($BaTiO_3$) single crystals are used to identify several of the structures. Examples of all eight structures can be found in the literature, either in micrographs or model predictions. The methods used to identify the full set are readily applied to other material systems; this is illustrated using the polar rhombohedral system as an example.

II. THEORY

A. Domain compatibility and tree diagram

There are six crystal variants in the polar tetragonal crystal system. Number these variants 1,...,6 corresponding to the six polarization directions $\hat{\mathbf{p}} = \pm[1,0,0], \pm[0,1,0], \pm[0,0,1]$, respectively. Each crystal variant has a corresponding eigenstrain $\boldsymbol{\epsilon}$ of the form

$$\boldsymbol{\epsilon} = \epsilon_0\left(\hat{\mathbf{p}} \otimes \hat{\mathbf{p}} - \tfrac{1}{3}\mathbf{I}\right), \tag{1}$$

where ϵ_0 is a crystal parameter, and strains are referred to a cubic reference state of equal volume; $\mathbf{I}$ is the 3×3 identity matrix. A domain is a region with uniform eigenstrain and polarization. Now, consider a pair of domains i and j with strain states $\boldsymbol{\epsilon}_i, \boldsymbol{\epsilon}_j$ and polarization states $\mathbf{p}_i, \mathbf{p}_j$. The normal $\mathbf{n}$ to the domain wall separating domains i and j is required to satisfy the well-known compatibility equations:[4,21]

$$\boldsymbol{\epsilon}_i - \boldsymbol{\epsilon}_j = \tfrac{1}{2}(\mathbf{a} \otimes \mathbf{n} + \mathbf{n} \otimes \mathbf{a}), \tag{2}$$

$$(\mathbf{p}_i - \mathbf{p}_j) \cdot \mathbf{n} = 0 \tag{3}$$

for some vector $\mathbf{a}$. Equation (2) has solutions of the form:[22]

$$\mathbf{n} = \frac{\mathbf{e}_2 \pm \mathbf{e}_1}{\sqrt{2}}, \tag{4}$$

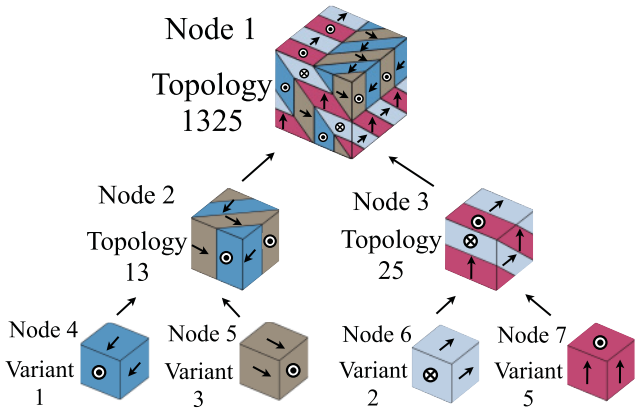

FIG. 1. (Color online) Rank-2 tree diagram representing the domain pattern 1325.

where $\mathbf{e}_1$ and $\mathbf{e}_2$ are eigenvectors of the matrix $\mathbf{M} = \boldsymbol{\epsilon}_i - \boldsymbol{\epsilon}_j$ with eigenvalues $\lambda_1 = -\lambda_2$ and $\lambda_3 = 0$. Applying Eq. (3) produces a unique interface normal when $\mathbf{p}_i \perp \mathbf{p}_j$, giving a 90° domain wall. In the special case when $\mathbf{p}_i \parallel \mathbf{p}_j$, Eq. (2) is trivially satisfied, and Eq. (3) provides a continuous set of solutions for interface normal $\mathbf{n}$. This gives 180° domain walls, which have no habit plane and result in "watermark" domain patterns.[1]

The relationship between the components of a periodic, rank-2 laminate can be described by a tree diagram.[36] Figure 1 shows a rank-2 tree diagram containing 7 nodes ($k = 1, \ldots, 7$). The material represented by node k has volume fraction f_k. If a node is not in the lowest level of the tree, it connects to exactly two child nodes, and its volume fraction is the sum of the volume fractions at the child nodes. Each node also has average strain and polarization values given by the volume average of those in its child nodes. All parent nodes are associated with an interface normal vector $\mathbf{n}_k$ that indicates the orientation of the compatible domain wall between the materials represented by its child nodes. Node number 1 (the root node) represents the entire laminate structure.

Nodes 4–7, in the lowest level of the tree, represent pure crystal variants, each of which is labeled by its variant number. For clarity, we introduce a simple way to distinguish and label laminate structures, using the variant numbers in the lowest level of the tree diagram. For example, the rank-2 laminate in Fig. 1 is labeled "1325," while the rank-1 laminate represented by node 2 is labeled "13," and similarly node 3 is labeled "25." It is worth noting that the tree diagram specifies a pattern or topology of domains. To describe a real structure, the physical size of the layers is needed, and this can be achieved by associating a domain wall spacing l_k with each parent node. Changing the domain wall spacings can make a significant difference to the appearance of a laminate without altering its topology, as shown in Fig. 2(b).

We can identify whether a rank-2 laminate domain structure satisfies exact compatibility conditions by examining its tree diagram.[22] Condition (i) for exact compatibility requires matching of domain wall spacings. In the rank-2 case, this is achieved by matching the volume fraction ratios $f_4/f_5 = f_6/f_7$ and length scales $l_2 = l_3$ regardless of topology. Condition (ii) requires that the projection of each domain wall normal onto the higher level interface must match that

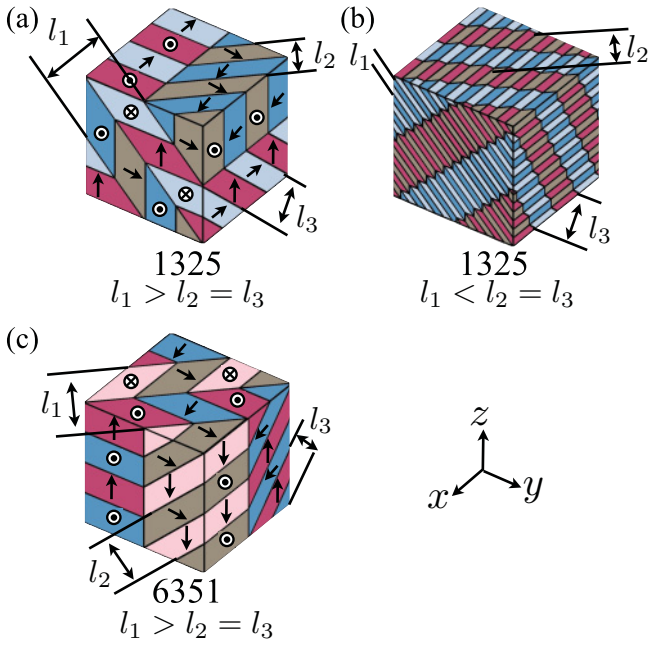

FIG. 2. (Color online) Equivalent domain topologies. (a) Structure 1325. (b) Structure 1325 with domain spacing $l_1 < l_2 = l_3$. (c) Structure 6351 is a rigid rotation of 1325 by 90° about the y axis.

of the corresponding domain wall on the opposite side of the interface. By a "higher level" interface, we mean a domain wall whose normal vector is associated with a higher rank lamination. For example, when two rank-1 laminations are combined to form a rank-2 laminate, the interface separating the two rank-1 laminates is a higher level interface. Condition (ii) is satisfied if and only if the interface normals of nodes 1, 2, and 3 are coplanar,[22] that is $\mathbf{n}_1 \cdot (\mathbf{n}_2 \times \mathbf{n}_3) = 0$. A similar condition was given by Fousek and Mokry.[37] Finally, Condition (iii) requires that every domain wall must satisfy Eqs. (2) and (3). In a rank-2 tree diagram, nodes 4, 5 and nodes 6, 7 must be compatible across interface normals $\mathbf{n}_2$ and $\mathbf{n}_3$, respectively; also nodes 4, 6 and nodes 5, 7 must be compatible across interface normal $\mathbf{n}_1$. Given the set of crystal variants in the lowest level of the tree diagram, Conditions (ii) and (iii) give rise to a total of nine vector equations for the three interface normals $\mathbf{n}_1$, $\mathbf{n}_2$, and $\mathbf{n}_3$. Thus, the system of equations is greatly over constrained, and solutions exist only for particular combinations of crystal variants. The set of solutions is found below.

B. Set of exactly compatible rank-2 laminates

To find the set of distinct rank-2 laminate domain structures in the polar tetragonal system, note that there are six crystal variants, giving $6^4 = 1296$ possible arrangements in the lowest level of the tree diagram. However, permutations that exchange all node pairs in any level of the tree give identical topology, e.g., $1325 \equiv 3152 \equiv 2513 \equiv 5231$. Next, remove rigid rotations, reflections, and inversions according to the symmetry operations that leave the set of six polarization vectors invariant. For example, Fig. 2(c) shows that 1325 and 6351 have equivalent domain topologies since 6351 is a rigid rotation of 1325 by 90° about the y axis. Those symmetry operations are the elements of the $m3m$ symmetry group. This leaves only the 24 distinct topologies listed in Table I.

TABLE I. Twenty-four distinct topologies of a rank-2 laminate made of polar tetragonal crystal variants, showing the subset of eight exactly compatible rank-2 laminates.

Not exactly compatible	Rank < 2, exactly compatible	Rank = 2, exactly compatible
1123	1111	1112
1134	1113	1213
1135	1122	1221
1223	1133	1234
1235	1212	1314
1315	1313	1324
1332	1331	1325
1335		1342
1345		

Now check if the 24 distinct topologies can satisfy Conditions (ii) and (iii) for exactly compatible rank-2 laminates. The compatibility equations contain nonlinearity and degeneracy; an effective solution strategy was found by first solving for *average* compatibility, and then testing each averagely compatible solution for exact compatibility. Average compatibility is achieved if the compatibility equations can be solved for node pairs (4,5), (6,7), and (2,3). In the case of node pair (2,3), the strain and polarization states to be used in Eqs. (2) and (3) are the volume averages of those in their child nodes. The existence of an averagely compatible solution can be shown to be independent of the choice of volume fractions $f_4, \ldots, f_7$, provided $f_4/f_5 = f_6/f_7$. The degenerate 180° domain walls that give a nonunique normal $\mathbf{n}$ are dealt with by changing the solution order and using the coplanarity condition. This procedure identifies nine domain topologies that violate the exact compatibility conditions as shown in the first column of Table I. Also, seven topologies have all domain walls parallel, and so reduce to laminates of rank less than 2. Finally, eight topologies satisfy the exact compatibility conditions and are of rank 2—see Table I.

Schematic unit cells of these eight types of domain pattern are shown in Fig. 3, where the notation $\{\cdots\}$ is used to represent families of symmetry related patterns. It is worth noting that the domain walls marked with dashed lines in Fig. 3 indicate 180° domain walls which can curve to form watermark domain patterns. However, some 180° domain walls in Fig. 3 are constrained by the 90° domain walls they meet. This phenomenon was also observed by Hu *et al.*[2] Where the pattern of laminations forces two regions of material of the same crystal variant to meet, there is no domain wall, but fictitious domain walls are included in Fig. 3 to aid visualization of the periodic laminate structure.

The patterns in the $\{1112\}$ and $\{1221\}$ families have only two crystal variants present, separated by 180° walls. The only distinction between these patterns is whether the domain walls cross, as in $\{1221\}$, or form closed loops, as in $\{1112\}$. It is interesting to note that four families, $\{1213\}$, $\{1234\}$, $\{1314\}$, and $\{1325\}$, show herringbone patterns on at least one surface. However, all patterns except $\{1325\}$ can show stripes of

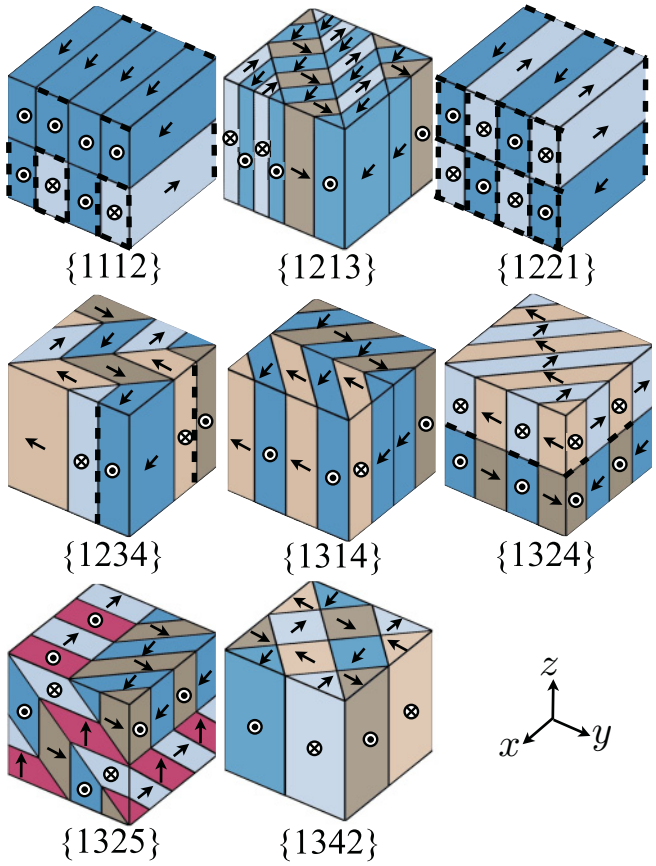

FIG. 3. (Color online) Unit cells of the eight exactly compatible, periodic, rank-2 laminate domain patterns.

domains at a surface. This presents considerable ambiguity in identifying domain patterns from surface images. Only family {1325} among these eight types has both in-plane and out-of-plane polarization directions present. Thus, the resulting domain structure is the most three-dimensional among the exactly compatible rank-2 laminates. Finally, family {1342} takes the form of an array of polarization vortices with alternating sense. These domain patterns can all be considered as minimum energy states within the constrained theory. Note, however, that the formation of several of the patterns from a high symmetry cubic state results in the presence of disclinations at the junctions of domain walls. Tsou and Huber[22] gave a method to check laminate domain patterns for the presence of disclinations. Using this method, we find that patterns {1213} and {1314} contain disclinations of magnitude $2(c-a)/a$ at the domain junctions, where a and c are lattice parameters. Pattern {1342} has disclinations of magnitude $4(c-a)/a$. Pattern {1325} also has a disclination, though its magnitude is only $\sim 0.8(c-a)^2/a^2$; the other patterns are disclination free.

To illustrate the applicability of the methods described here, rank-2 laminates in the polar rhombohedral crystal system were classified by the same method. In this system, there are eight crystal variants; number them $1,\ldots,8$ with polar directions $\sqrt{3}\hat{\mathbf{p}} = \pm[1,1,1], \pm[-1,1,1], \pm[-1,-1,1]$, and $\pm[1,-1,1]$, respectively. The corresponding eigenstrains, measured from an equal volume reference state, are given by Eq. (1). The 8^4 permutations of the rank-2 tree reduce using the $m3m$ symmetries to 51 distinct topologies of which only 14 are distinct exactly compatible patterns not equivalent to a lower rank structure, as listed in Table II. Patterns {1342} and {1432} have identical topology, arising from a coincidence of domain wall orientations $\mathbf{n}_2 \equiv \mathbf{n}_3$ in both patterns. Some of the patterns in Table II have been found by other methods; for example, a rhombohedral {1357} laminate was predicted using phase-field methodology by Shu *et al.*[38] Our method provides an extremely rapid and complete identification of minimum energy laminates. The method is readily extended to higher rank laminates, though the number of patterns becomes large and laminates of rank greater than 2 are less commonly observed in ferroelectric crystals. Applications to nonpolar systems, such as shape memory alloys, also reveals interesting structures, and will be described elsewhere.

TABLE II. Fifty-one distinct topologies of a rank-2 laminate made of polar rhombohedral crystal variants, showing the subset of exactly compatible rank-2 laminates.

Not exactly compatible	Rank < 2, exactly compatible	Rank $= 2$, exactly compatible
1123 1223	1111	1112
1124 1224	1113	1213
1134 1315	1114	1214
1135 1316	1122	1221
1136 1332	1133	1234
1145 1335	1144	1243
1235 1336	1212	1314
1236 1346	1313	1324
1246 1368	1331	1325
1326 1415	1414	1342(1432)
1345 1436	1441	1357
1358 1445		1423
1467		1426
		1458

III. OBSERVATIONS OF TETRAGONAL RANK-2 LAMINATES

Each of the tetragonal structures described in Sec. II has been reported in the literature, either as the result of direct observation, or from theoretical considerations. In this section, evidence for the formation of rank-2 domain structures is given, predominantly by comparing the patterns in Fig. 3 with similar patterns found in the literature. Additionally, we used a variety of standard imaging techniques, including scanning electron microscopy (SEM), atomic force microscopy (AFM), piezoresponse force microscopy (PFM), and optical microscopy to find examples of several of these structures in an unpoled tetragonal barium titanate single crystal. Examples are shown in Fig. 4.

Figure 4(a) shows a watermark domain pattern with antiparallel out-of-plane polarization directions found in a $BaTiO_3$ single crystal, etched using 10% HF aqueous solution for 20 s. The image was generated using a Zeiss EVO LS 15 ESEM in secondary electron mode, with a 10-keV beam

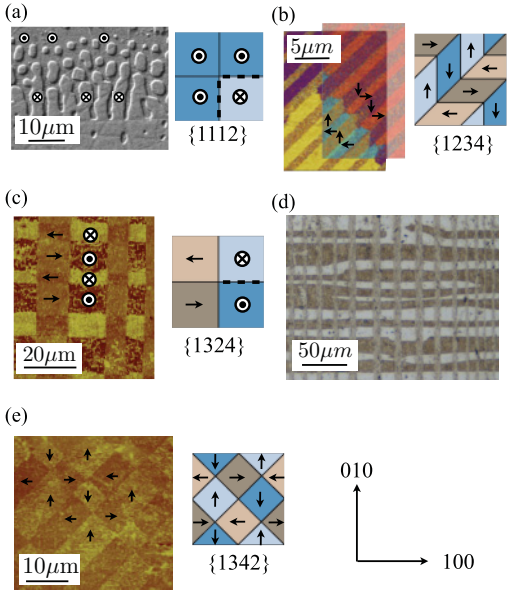

FIG. 4. (Color online) SEM, PFM, AFM, and optical microscopy used to show rank-2 laminate domain patterns in tetragonal barium titanate: (a) {1112}, (b) {1234}, (c) and (d) {1324}, and (e) {1342}.

and 7 mm working distance. This illustrates a {1112} type structure in which domain walls are curved. A corresponding surface of the {1112} unit cell is shown. The {1221} type structure, with crossing 180° domain walls, was not found in our crystals, and experimental observations appear to be rare. A possible explanation is that the crossing domain walls in {1221} can separate, merging the regions into closed domain loops and, thus, transforming the pattern into the {1112} type. This would reduce the overall domain wall energy. There are several reported observations of {1112} type structure,[39–41] and the {1221} type is also illustrated in the literature.[42]

Figure 4(b) shows the domain pattern in an unetched $BaTiO_3$ single crystal, obtained by lateral PFM, that allows mapping of in-plane piezoelectric distortions, and hence, the polarization vector direction.[43] An Asylum Research MFP-3D AFM system in piezoresponse mode was used, with an Olympus AC240TM cantilever. The scan rate was 1 Hz, driving voltage 4.4 V, and frequency 885 kHz was used to give contact resonance. In Fig. 4(b), domain pattern {1234}, with four distinct in-plane domain types in a herringbone arrangement, is revealed by overlapping the results from two orthogonal PFM scans. Note that the observed structure cannot be any of the other herringbone patterns as PFM reveals four in-plane domain types. This structure was also reported in a recent PFM study by McGilly *et al.*[44] and is a well-known arrangement of tetragonal domains.[5,7,41,45]

Figures 4(c) and 4(d) show checkerboard domain patterns in etched $BaTiO_3$, imaged by AFM and optical microscopy, respectively. The AFM image was obtained using a Veeco Dimension 3100 AFM system with Nanoscope III D Controller. SCM-PIC tips were used in contact mode at a scan rate of 1 Hz, revealing a topographic contrast of about 100 nm caused by etching. Square checks appear in patterns {1221}, {1324}, and {1342}, but here, alignment of the checks to the crystallographic axes eliminates {1342} and makes {1221} unlikely. The difference in etching depth between the in-plane and out-of-plane domains confirms this as pattern {1324}. It is interesting to note that the two sublaminates (13 and 24) are separated by a 180° domain wall that alternates between fixed orientation and flexible orientation as it crosses the pattern, resulting in curved domain walls between the crystal variants polarized in the out-of-plane direction. Thus, the {1324} structure can form a watermark pattern intersected by straight 90° domain walls as shown in Fig. 4(d), which was produced by viewing an etched $BaTiO_3$ crystal using an Alicona InfiniteFocus microscope. Similar domain configurations have been reported in previous work.[40,46]

The {1342} pattern exhibits an array of polarization vortices, a structure that has been predicted using diffuse interface models.[31,47] However, the pattern has not been widely observed, perhaps due to the strong disclinations present, which make this a relatively high energy state. The pattern has also been shown to be unstable to an electric field except in the presence of stress.[45] The AFM image of etched barium titanate shown in Fig. 4(e) was generated using the same method as Fig. 4(c) on a different sample of barium titanate. This appears to reveal the {1342} domain pattern, containing 90° domain walls in a checkerboard pattern oriented at 45° to the crystallographic axes. Relatively low contrast between the domains was achieved, as expected for the etching of in-plane domains.

Finally, patterns in the {1325} family have been widely observed and discussed.[1–3,5,10,12,21,30] All the domain walls, including the 180° walls, in this pattern have orientations fixed by the requirements of compatibility. Domain patterns of {1213} and {1314} were not found in our sample, but have been discussed in the literature.[42]

IV. CONCLUSION

In this paper, three-dimensional compatibility conditions were defined and used to classify compatible domain patterns in ferroelectric single crystals. It was found that there are remarkably few distinct domain arrangements that can form as compatible laminates. The eight types of periodic exactly compatible rank-2 laminates are defined and examples from simulation and observations confirm their existence. While each of the eight patterns in the tetragonal system had already been described, there does not appear to be a systematic classification in previous works. Major advantages of the method developed here are the rapidity and completeness of finding minimum energy patterns. A further advantage is the ease with which the method can be extended to other crystal systems or higher rank laminates. The resulting classification is of direct use in identifying observed domain patterns and provides a basis to search for engineered domain configurations with optimized properties.

ACKNOWLEDGMENTS

The authors wish to acknowledge the support of EPSRC, Project No. EP/E026095/1.

*nien-ti.tsou@eng.ox.ac.uk
†prashant.potnis@eng.ox.ac.uk
‡john.huber@eng.ox.ac.uk

[1]G. Arlt and P. Sasko, J. Appl. Phys. **51**, 4956 (1980).
[2]Y. H. Hu, H. M. Chan, Z. X. Wen, and M. P. Harmer, J. Am. Ceram. Soc. **69**, 594 (1986).
[3]G. Arlt, J. Mater. Sci. **25**, 2655 (1990).
[4]J. Li and D. Liu, J. Mech. Phys. Solids **52**, 1719 (2004).
[5]J. Rodel, Mech. Mater. **39**, 302 (2007).
[6]S. Choudhury, L. Q. Chen, and Y. L. Li, Appl. Phys. Lett. **91**, 032902 (2007).
[7]G. J. Weng and D. T. Wong, J. Mech. Phys. Solids **57**, 571 (2009).
[8]J. H. Yen, Y. C. Shu, J. Shieh, and J. H. Yeh, J. Mech. Phys. Solids **56**, 2117 (2008).
[9]E. Burcsu, G. Ravichandran, and K. Bhattacharya, J. Mech. Phys. Solids **52**, 823 (2004).
[10]A. L. Roitburd, Phys. Status Solidi A **37**, 329 (1976).
[11]S. P. Alpay and A. L. Roytburd, J. Appl. Phys. **83**, 4714 (1998).
[12]A. L. Roytburd, S. P. Alpay, L. A. Bendersky, V. Nagarajan, and R. Ramesh, J. Appl. Phys. **89**, 553 (2001).
[13]Y. L. Li, S. Y. Hu, Z. K. Liu, and L. Q. Chen, Acta Mater. **50**, 395 (2002).
[14]J. S. Speck and W. Pompe, J. Appl. Phys. **76**, 466 (1994).
[15]A. L. Roytburd, J. Appl. Phys. **83**, 228 (1998).
[16]N. A. Pertsev and V. G. Koukhar, Phys. Rev. Lett. **84**, 3722 (2000).
[17]Y. L. Li, S. Y. Hu, Z. K. Liu, and L. Q. Chen, Appl. Phys. Lett. **78**, 3878 (2001).
[18]K. J. Choi, M. Biegalski, Y. L. Li, A. Sharan, J. Schubert, R. Uecker, P. Reiche, Y. B. Chen, X. Q. Pan, V. Gopalan, L. Chen, D. G. Schlom, and C. B. Eom, Science **306**, 1005 (2004).
[19]N. T. Tsou and J. E. Huber, Continuum Mech. Thermodyn. **22**, 203 (2010).
[20]J. M. Ball and R. D. James, Arch. Ration. Mech. Anal. **100**, 13 (1987).
[21]Y. C. Shu and K. Bhattacharya, Philos. Mag. Part B **81**, 2021 (2001).
[22]N. T. Tsou and J. E. Huber, Mech. Mater. **42**, 740 (2010).
[23]E. Fried and M. E. Gurtin, Physica D: Nonlinear Phenomena **68**, 326 (1993).
[24]E. Fried and M. E. Gurtin, Physica D: Nonlinear Phenomena **72**, 287 (1994).
[25]Y. Su and C. M. Landis, J. Mech. Phys. Solids **55**, 280 (2007).
[26]H. L. Hu and L. Q. Chen, J. Am. Ceram. Soc. **81**, 492 (2005).
[27]W. Cao and L. E. Cross, Phys. Rev. B **44**, 5 (1991).
[28]J. Wang, S. Q. Shi, L. Q. Chen, Y. Li, and T. Y. Zhang, Acta Mater. **52**, 749 (2004).
[29]L. M. Eng, J. Fousek, and P. Gunter, Ferroelectrics **191**, 419 (1997).
[30]S. Y. Cheng, N. J. Ho, and H. Y. Lu, J. Am. Ceram. Soc., **89**, 2177 (2006).
[31]D. Schrade, R. Mueller, B. Xu, and D. Gross, Comput. Methods Appl. Mech. Eng. **196**, 4365 (2007).
[32]N. Balke, S. Choudhury, S. Jesse, M. Huijben, Y. H. Chu, A. P. Baddorf, L. Q. Chen, R. Ramesh, and S. V. Kalinin, Nat. Nanotechnol. **4**, 868 (2009).
[33]V. Anbusathaiah, S. Jesse, M. Arredondo, F. Kartawidjaja, O. Ovchinnikov, J. Wang, S. Kalinin, and V. Nagarajan, Acta Mater. **58**, 5316 (2010).
[34]V. Anbusathaiah, D. Kan, F. C. Kartawidjaja, R. Mahjoub, M. A. Arredondo, S. Wicks, I. Takeuchi, J. Wang, and V. Nagarajan, Adv. Mater. **21**, 3497 (2009).
[35]S. Wicks, K. Seal, S. Jesse, V. Anbusathaiah, S. Leach, R. E. Garcia, S. V. Kalinin, and V. Nagarajan, Acta Mater. **58**, 67 (2010).
[36]G. H. Goldsztein, J. Mech. Phys. Solids **49**, 899 (2001).
[37]J. Fousek and P. Mokry, Ferroelectrics **323**, 3 (2005).
[38]Y. C. Shu, J. H. Yen, H. Z. Chen, J. Y. Li, and L. J. Li, Appl. Phys. Lett. **92**, 052909 (2008).
[39]L. Jin, Ceramics International **30**, 1695 (2004).
[40]J. Fousek and M. Safrankova, Jpn. J. Appl. Phys. **4**, 403 (1965).
[41]J. Hooton and W. Merz, Phys. Rev. **98**, 409 (1955).
[42]A. K. Tagantsev, L. E. Cross, and J. Fousek, *Domains in Ferroic Crystals and Thin Films* (Springer, New York, 2010).
[43]S. V. Kalinin, B. J. Rodriguez, S. Jesse, E. Karapetian, B. Mirman, E. A. Eliseev, and A. N. Morozovska, Annu. Rev. Mater. Res. **37**, 189 (2007).
[44]L. J. McGilly, A. Schilling, and J. M. Gregg, Nano Lett. **10**, 4200 (2010).
[45]N. T. Tsou and J. E. Huber, in *Behavior and Mechanics of Multifunctional Materials and Composites 2010*, edited by Z. Ounaies and J. Li (SPIE, San Diego, 2010), p. 76440B.
[46]Y. Cho, S. Kazuta, K. Matsuura, and H. Odagawa, J. Eur. Ceram. Soc. **21**, 2131 (2001).
[47]I. I. Naumov, L. Bellaiche, and H. Fu, Nature **432**, 737 (2004).